Research Article

BIOMEDICAL Journal of Scientific & Technical Research

ISSN: 2574 -1241

DOI: 10.26717/BJSTR.2022.42.006749

# Preclinical Evaluation of $^{124}$I-Radionuclide for PET/CT Imaging System

**Sitah Fahad Alanazi[1]*, Salem Ahmed Sassi[2], Ibrahim Jammaz Aljammaz[3] and Yousif Hassan ALmalki[3]**

[1]*Imam Mohammad ibn Saud Islamic University (IMSIU), College of Science, Department of Physics, Saudi Arabia*

[2]*Department of Medical Physics, Prince Sultan Military Medical City, Saudi Arabia*

[3]*Cyclotron and Radiopharmaceuticals Department, King Faisal Specialist Hospital and Research Center, Saudi Arabia*

***Corresponding author:** Sitah F Alanazi, Imam Mohammad Ibn Saud Islamic University (IMSIU), College of Science, Department of Physics, Riyadh 11642, Saudi Arabia

**ARTICLE INFO**

**Received:** February 19, 2022

**Published:** March 08, 2022

**Citation:** Sitah Fahad Alanazi, Salem Ahmed Sassi, Ibrahim Jammaz Aljammaz, Yousif Hassan ALmalki. Preclinical Evaluation of $^{124}$I-Radionuclide for PET/CT Imaging System. D-154. Biomed J Sci & Tech Res 42(3)-2022. BJSTR. MS.ID.006749.

**ABSTRACT**

124-Iodine ($^{124}$I) is an attractive radionuclide in clinical and preclinical PET imaging studies with a long half-life of 4.2 days. $^{124}$I has specific physical characteristics that make it more suitable than the more conventional PET radionuclides. The aim of this study is to evaluate some quantitative imaging characteristics of $^{124}$I-PET using a small animal Nano Scan PET/CT system and comparing these results with those obtained for $^{18}$F and $^{89}$Zr.

**Methods**: The system's spatial resolution, uniformity, and image quality were measured on a Nano Scan small-animal PET/CT scanner according to the NEMA NU4-2008 protocols. For reconstruction images, we used 2D and 3D reconstruction algorithms. The reconstruction methods included filter back projection (FBP)and the 3D Tera-Tomo algorithm, which are developed for the NanoScan small-animal PET/CT scan.

**Result**: The long mean positron ranges of $^{124}$I (3.48 mm) caused a significantly low resolution (high value of FWHM) as compared with $^{89}$Zr and $^{18}$F, it was 1.7mm for$^{124}$I where this value was 0.9 and 1 mm for $^{18}$F and $^{89}$Zr, respectively. The spillover ratio (SORs) values were the highest value in water filled compartment for $^{18}$F, while they were close to each other for $^{124}$I and $^{89}$Zr. On the other hand, in the case of air filled compartment the results have shown no significant difference. The results of recovery coefficient (RC) values have shown a significant reduction was observed for $^{124}$I. The high differences in the SOR and significant reduction in RCs were observed for $^{124}$I as compared to $^{89}$Zr and $^{18}$F. Best results were found for $^{18}$F.

**Conclusion**: In this study the image quality parameters and spatial resolution were evaluated for $^{124}$I using small animal NanoScan® PET/CT scanner. We have considered the main problems that can limit the image quality performance is the higher positron range and the presence of prompt ɣ-photons. The presence of ɣ-photons effects on the image quality parameters for high positron range, particularly SD%.

## Introduction

In recent years, PET/CT is considered as an essential multimodality imaging that commonly used in oncology due to its ability to providing both anatomical and functional information. PET/CT has an important value in the detection and staging of several types of cancer. It can improve cancer diagnosis and follow-up the assessment of tissues response to treatment. The PET/CT imaging can help in detection of small lesions. These developments are showing dramatically in the advance generations of PET/CT which include new software, hardware, and acquisition methods [1], for example it introduces some new image reconstruction methods such as time –of- flight (TOF), a continuous bed motion and combined PET with other modalities. These growths in PET/CT can influence on cancer imaging as the can produce better image quality and more accurate details of therapy monitoring and uptake [1]. Fluorine -18 ($^{18}$F) is considered as a gold standard positron emitter in PET imaging, it has a widely uses in imaging applications when it is labelled with some pharmaceutical compounds such as $^{18}$F-fluorodeoxyglucose (FDG),$^{18}$F-fluoromisonidazole,$^{18}$F-fluoroazomycin-arabinoside, and $^{18}$F-fluoro-3'-deoxy-3'-L-fluorothymidine. Nowadays, PET imaging plays an important role in radioimmunotherapy (RIT) which known as Immuno-PET and it is used to estimate cancer treatment with monoclonal antibodies (mAbs) [2].

The best radionuclides for these applications should has a physical half-life matches the biological half-life of antibodies (mAbs) or pharmaceutical molecules in circulation, so that other positron emitters with half-life greater than 48h are being used such as $^{124}$I ,$^{89}$Zr and Y90 [3]. Each of these isotopes has different physical characteristics for instance positron energies, positron ranges and fraction of single photons emitted [3]. The long physical half-life of I-124 which is about 4.2 days make it suited in vivo studies. Despite this optimal characteristic for matching with mAbs, two main features can be expected to limit the image resolution in in preclinical PET imaging, one is the high energy and therefore long range of the emitted positrons. Pre-clinical imaging on animals are critical tools to explore multi-scale variations i.e. from organ, tissue, cell, down to molecular levels, resulted due to physiological, pathological or pharmacological changes, Precedes to human study human clinical trials. Rapid development in PET systems can permit the translation of large scale PET imaging (which used in human and large animals) abilities to the scale of small animals by using small-animal PET [4]. The use of small animal imaging has become an effective key in translational research, it is considered as a bridge between developments in vitro studies and clinical applications in diagnosis and/or therapeutics [5].

Some of disadvantages include the high positron energy and large positron range in tissue (e.g., $^{68}$Ga and $^{124}$I) may effect on the spatial resolution of the image and produce low spatial resolution and recovery coefficient (RC). Similarly, the presence of single ɣ photons (e.g., $^{124}$I and $^{89}$Zr) can have undesirable effects on the image quality, it might increase image noise and spillover ratios (SORs). The purpose of this study was to compare some of performance parameters such as image quality and spatial resolution of $^{18}$F, $^{124}$I and $^{89}$Zr using small animal Nano-Scan PET/CT.

## Materials and Methods

### PET/CT Scanner

The NanoScan PET/CT system is used (Mediso Ltd) (Figure 1), which has a high sensitivity, high resolution and fully integrated small-animal PET/CT system. The axial field-of-view (FOV) of the PET ring is 10 cm. The PET system has 12 detector blocks of 81×39 Lutetium Yttrium Orthosilicate (LYSO) crystals (1.12 mm×1.12 mm×13.0 mm), tightly packed (pitch 1.17 mm, packing fraction 92%) coupled to two 256-channel position sensitive photomultiplier tubes. The detector blocks are mounted in rings of diameter $^{18}$4 mm, and there are 2 rings in total. Each detector block is connected with 1, 3, or 5 blocks on the opposite direction of the ring for coincidence detection (coincidence mode 1:1, 1:3 and 1:5). The CT system is a cone-beam CT scanner. It has a flat panel CMOS detector of 15×12 cm$^2$ $Gd_2O_2S$. The maximum current of X-ray tube is 0.18 mA, the tube voltage ranges from 30 to 80 kVp and the tube power is 50/80 W. PET data are sorted in list mode format and for image reconstruction several options can be used; filtered Back-projection (FBP), 3D projection, 2D and 3D ordered-subset expectation maximization (OSEM2D and OSEM3D, respectively). A fully 3-dimensional (3D) reconstruction using a Tera-Tomo algorithm (Tera-Tomo; Mediso Ltd.), all image quality factors are achieved for at least 30 min acquisition and image reconstruction with 52 iterations which is the default image reconstruction method of NanoScan PET/CT, also used. A multiple Graphical Processing Unit (GPUs) are used for CT reconstruction. Reconstruction is done using filtered back-projection method, with following available filters; RamLack, Hamming, Hann, Shepp-Logan, Butterworth, Cosine and BlackMan.


**Figure 1:** The Mediso NanoScan® PET/CT system with description.

## Radionuclides

The radionuclides used in this study are $^{18}F$ $^{124}I$ and $^{89}Zr$. The main physical properties of these radionuclides are present in (Table 1). $^{18}F$ is most commonly used in PET scan which is used for early detection of tumors and evaluation of response to cancer therapy. Moreover,$^{18}F$ is an essential isotope for standard measurements of PET acceptance tests suggested by NEMA NU. Today, the two others radionuclides, $^{124}I$ and $^{89}Zr$, are increasingly used in PET. $^{124}I$ is a radionuclide with positron abundance of approximately 23%, about 50% of all positrons are emitted simultaneously with a 603-keV gamma photon a high positron energy and a high abundance of singles. $^{124}I$ has dual energy emission: beta radiation emissions of 1532 keV (11%) and 2135 keV (11%) and gamma emissions of 511 keV (46%), 603 keV (61%), and 1691 keV (11%). $^{89}Zr$ is a neutron deficient isotope of Zirconium with 49 neutrons and 40 protons, and it decays with a half-life of 3.27 days to $^{89}Y$. The decay proceeds via electron capture (77%), and positron emission (23%). Both modes of decay lead primarily (99%) to a 9/2+ state in $^{89}Y$, which de-excites through M4 emission of a 909 keV gamma ray to the 1/2- ground state. Therefore, the important decay radiations are the 511 keV γ's from positron annihilation, the 909 keV γ from the $^{89m}Y$ de-excitation, continuum positrons (23% endpoint = 902 keV), internal conversion electrons from the M4 transition (0.8%), and Auger electrons. The prompt photons fall outside the default energy window, apart from a portion of the down-scattered photons with lower energy.

**Table 1:** Physical properties of $^{18}F$, $^{89}Zr$ and $^{124}I$ [5].

| Property | $^{18}F$ | $^{89}Zr$ | $^{124}I$ |
|---|---|---|---|
| Half-life | 109.8 min | 3.27 d | 4.18 d |
| $\beta^+$ yield | 0.97 | 0.23 | 0.23 |
| Mean $\beta^+$ energy (MEV) | 0.25 | 0.40 | 0.83 |
| Mean $\beta^+$ range in water (mm) | 0.62 | 1.23 | 3.48 |
| Single γ-yield in range of 350-650 keV | 0.00 | 0.00 | 0.64 |
| Single γ-yield outside range of 350-650 keV | 0.00 | 0.99(909.2 keV) | 0.10(722.8 keV)<br>0.19 (>1.5 MeV) |

Their high yield (0.99 ɣ-photons vs. 0.23 positrons) could contribute to the detector dead time [6]. Radionuclide production was carried out at King Faisal Specialist Hospital and Research Centre. $^{89}Zr$ was produced through the $^{89}Y$ (p, n) $^{89}Zr$ reaction by proton bombardment of $^{89}Y$ solid targets. Enriched Y2O3 targets in oxide form were prepared by hydraulically pressing (130–200 mg) $^{89}Y$ oxide powder (130–200 mg) into circular cavity aluminum target plates at 5000 psi. The $Y_2O_3$ targets were irradiated with accelerated protons at 90° to the cyclotron beam using a CS30 cyclotron (CTI Cyclotron Systems, Berkeley, California, USA) [4]. Irradiation times were between 2 and 3 h, energy was 15 MeV, beam current was 10 μA, and the $^{89}Zr$ yield obtained was around 8mCi. $^{89}Zr$ was isolated with high radionuclide and radiochemical purity (>99%) as $ZrCl_4$ using a solid-phase hydroxamate resin with more than 95% recovery of the radioactivity [4]. 24I was produced by the bombardment of enrich $^{125}Te$ targets (150 mg ±10%) with

18 MeV protons from the IBA Cyclon 30 using $^{125}Te(p,n)^{124}I$ nuclear reaction. The targets were prepared and processed by a standard operating procedure developed in-house. In brief, irradiated targets were dissolved in a mixture of sodium hydroxide (NaOH, 1.0 mL, 5.0 N), hydrogen peroxide ($H_2O_2$, 3.0 mL, 30 %) and de-ionized water (6.0 mL).

The dissolved $^{125}Te$ was transferred in 250 mL quartz reaction flask containing aluminum powder (160 mg) which was boiled until reaction is completed. Air was then bubbled through the solution for five minutes followed by bubbling of $CO_2$ for additional five minutes. The bubbled solution was then carefully filtered through a fine fritted glass and on-line AG50W-X8 column into pre-weighed serum vial. If necessary, the pH was adjusted in the range of 5-7 with NaOH (0.01 N). Finally, 0.6 mL of the $Na^{123}I$ bulk solution was subjected to quality control measures for radionuclidic purity, specific concentration, pH, tellurium and aluminum spot tests. Extracted $^{124}I$ was used immediately for radiopharmaceutical production [7].

## Spatial Resolution

The NEMA NU-2004 is specified to evaluate the spatial resolution for $^{22}Na$ only. For this reason, the transaxial spatial resolutions of the three radionuclides were measured using a new suggested method by us. For measuring the spatial resolution of $^{18}F$ and $^{89}Zr$ a point source was used. It was obtained by drilling a plastic plate to make a sphere with a radius less than 1 mm, and then it was filled with different isotopes. The activity was 3.37 MBq, 8.3 MBq and 0.32 MBq for $^{18}F$, $^{124}I$ and $^{89}Zr$, respectively, this difference in doses of isotopes is due to an availability issue. The activity was positioned in the center of the FOV, aligned with the axis of the scanner, and then put at 10 mm and 20 mm and scanned until at least 3.5 million counts were acquired using the default energy window of 250–750 keV and timing window of 3.432 ns. Images were obtained using FBP and the 3D Tera-Tomo algorithm, which are developed for the NanoScan small-animal PET/CT scanner with the default settings (ramp filter with a cutoff at Nyquist frequency) and 512 ×512 ×159 matrices with voxel sizes of 0.1 × 0.1×0.58 mm. This matrix size was selected to obtain a profile with a sufficient number of data points to allow for the accurate determination of spatial resolution all image quality factors is achieved for at least 30 min acquisition and image reconstruction with 52 iteration . No correction was applied, whether attenuation or scatter corrections. The reconstructed images were processed to measure full width at half and at tenth maximum (FWHM and FWTM, respectively) for the point source. According to the NEMA NU-4 standards, these widths were measured in parabolic fit through the peak pixel and its two nearest neighboring pixels. FWHM and FWTM were not corrected for source geometry [2].

## Image Quality

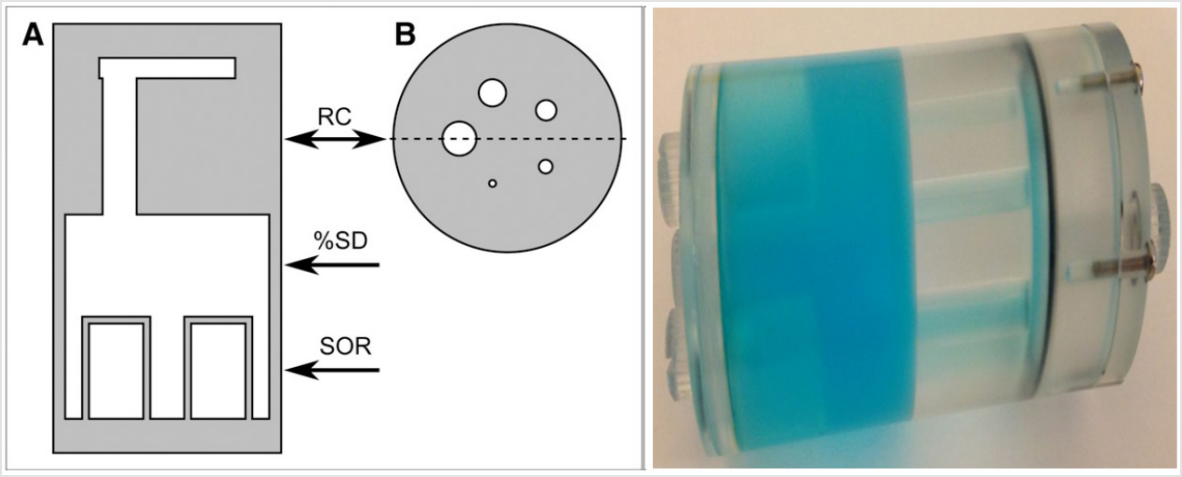


**Figure 2:** Cross-sectional diagram of NEMA NU-4 image quality phantom.

The image quality tests were done using NEMA image quality phantom (Figures 2 & 3), it is divided into three parts: the first region is a homogeneous block filled with radioactivity (30-mm diameter and 30-mm length) to determine the signal-to-noise ratio of the system. The second one consists of two chambers filled with cold water and air (length, 15 mm; outer diameter, 10 mm; wall thickness, 1 mm) to evaluate the scatter fraction in the image. The third part is a 5-rod region, these rods are used to calculate the recovery coefficient (RC) which is defined as the ratio between the measured activity concentration in the rods and the activity concentration measured in the uniform area [8]. The RC is theoretically limited between 1 and 0 ($0 < RC < 1$). A 2-cylinder-chamber region, one is filled with air, the other was filled with nonradioactive water, are used to measure the spillover

ratio (SOR) in water and air [2], which defined as the mean value in each cold cylinder divided by the mean in the uniform area and its theoretically value is range between 0 and 1 [2]. The percentage SD% which is considered as a measure of noise was determined by using the uniform region at the central of phantom. The phantom was filled with a specific isotope and the injected activity was 3.7 MBq. The scanning time was 20 minutes, a 5-ns time window and a 400-to-600 keV energy window. The measurement was performed in the normal-count mode of the scanner in 1:3 and 1:5 coincidence modes. In addition to the 2D-OSEM reconstruction image, the acquired data were reconstructed with default reconstruction algorithm of the system, Tera-Tomo reconstruction method. The image quality tests include; uniformity, recover coefficients and accuracy of correction.

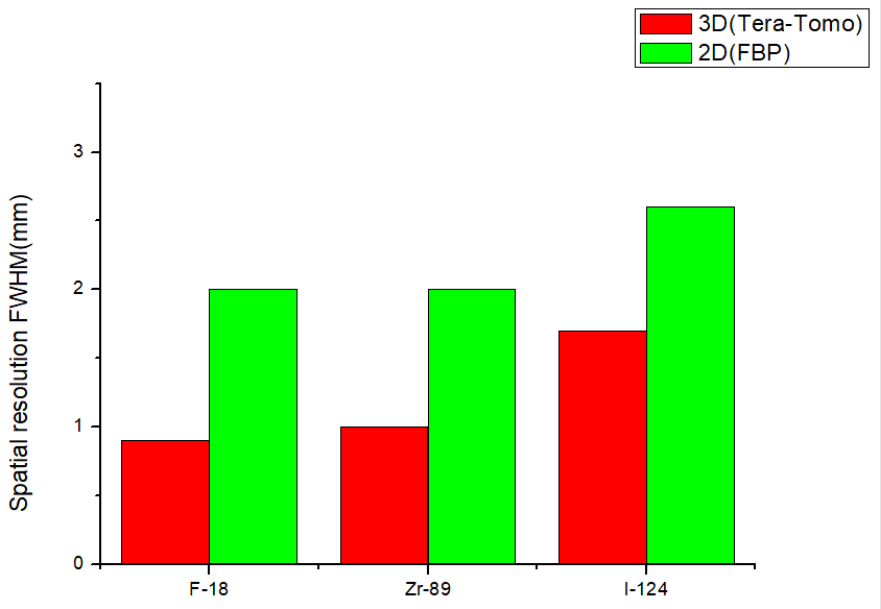


**Figure 3:** Spatial resolutions for 3 radionuclides measured with 3D-reconstruction and 2D- reconstruction.

## Results

In the following sections, the results for spatial resolution and image quality parameters are presented. The obtained values of three radionuclides are summarized in (Table 2).

### Spatial Resolution

The spatial resolution measurements using a point source of each radionuclide reconstructed with a Tera-Tomo 3D PET algorithm and with FBP-reconstruction image are presented in (Table 2). The spatial resolutions of tangential and radial direction at the center were averaged to calculate FWHM and FWTM. The FWHM were 0.9 mm, 1.0 mm and 1.7 mm for $^{18}$F, $^{89}$Zr and $^{124}$I, respectively, when using 3D-reconstruction method. While the spatial resolution values were lower when used FBP-reconstruction method, the FWHM values were 2.0 mm, 2.0 mm and 2.6 mm for $^{18}$F, $^{89}$Zr and $^{124}$I, respectively. According with Gaussian profile, the FWHM to FWTM ratio equal to $\sqrt{ln2/ln10}$ = 0.55, nongaussian profiles with extended tails are characterized by smaller FWHM-to-FWTM ratios [2]. Palmer, et al [9] and Disselhorst, et al [2] have measured spatial resolution and determined the corresponding FWHM to FWTM ratios, and they have showed that $^{18}$F have produced the best value of spatial resolutions and theoretic ratios (0.54 and 0.51 respectively). The data in Table 2 show that the

values of spatial resolution improve when using Tera-Tomo algorithm more than those in FBP algorithm for all isotopes, these values were 0.9, 1.0,and 1.7 mm for $^{18}$F, $^{89}$Zr and $^{124}$I, respectively. In addition, these data indicate that $^{18}$F provided the best values as compared to other isotopes (0.45) where the measured ratio of $^{89}$Zr (0.43, 0.5 and 0.5%, respectively) and for $^{124}$I (0.4, 0.39 and 0.41% respectively) are lower and we observed the same effect when we use 2D reconstruction (see Tables 2 & 3).

**Table 2:** Spatial resolutions for each radionuclide measured with Tera-Tomo and FPB reconstruction algorithm.

| radionuclide | FWHM(mm) | FWTM(mm) | FWHM to FWTM | Palmer et al | Disselhorst et al. |
|---|---|---|---|---|---|
| **Tera-Tomo 3D-reconstruction Algorithm** | | | | | |
| F-18 | 0.9 | 2.0 | 0.45 | 0.54 | 0.51 |
| Zr-89 | 0.1 | 2.3 | 0.43 | 0.50 | 0.50 |
| I-124 | 1.7 | 4.2 | 0.4 | 0.39 | 0.41 |
| **FPB- reconstruction Algorithm** | | | | | |
| F-18 | 2.0 | 4.6 | 0.43 | 0.54 | 0.51 |
| Zr-89 | 2.0 | 4.7 | 0.42 | 0.50 | 0.50 |
| I-124 | 2.6 | 6 | 0.43 | 0.39 | 0.41 |

**Table 3:** The SOR values of 3 different isotopes.

| **Spill Over Ratio (SOR)** | | | | | | |
|---|---|---|---|---|---|---|
| **Tear-Tomo 3D reconstruction** | | | | | | |
| **Components** | **SOR** | | | **%STD$_{SOR}$** | | |
| | **.$^{18}$F** | **$^{89}$Zr** | **$^{124}$I** | **.$^{18}$F** | **$^{89}$Zr** | **$^{124}$I** |
| Water filled chamber | 0.9 | 0.16 | 0.12 | 12.6 | 16.0 | 24.2% |
| Air filled chamber | 0.15 | 0.17 | 0.16 | 17.4 | 15.7 | 25.3% |
| **FBP 2D reconstruction** | | | | | | |
| **Components** | **SOR** | | | **% STD$_{SOR}$** | | |
| | **.$^{18}$F** | **$^{89}$Zr** | **$^{124}$I** | **.$^{18}$F** | **$^{89}$Zr** | **$^{124}$I** |
| Water filled chamber | 0.95 | 0.2 | 0.16 | 12.6 | 0.2 | 20.8 % |
| Air filled chamber | 0.23 | 0.23 | 0.11 | 15.2 | 0.23 | 19.9 % |

## Image Quality Results

### Uniformity

The %SD of the NEMA Nu-4 image-quality phantom is shown in (Figure 3). The largest differences are not obtained between $^{18}$F and $^{89}$Zr but it seems clear with$^{124}$I. Comparable values were obtained with F-18 and Zr-89, however I-124 showed a 47% higher value. For $^{124}$I, the % SD is greater than the values that were found for $^{18}$F and $^{89}$Zr. Moreover, among the different reconstruction algorithms for $^{124}$I there was a significant increase, where Tera-Tom yielded %SD value smaller than those obtained by FBP, it has shown 47% increase than those obtained by FBP.

### Accuracy of Corrections

The spill-over ratio (SOR) in cold regions is calculated to find the accuracy of activity correction. The spill-over ratio and STD % in the water- and air-filled cylinders are given in (Table 3). These results are obtained for 2D OSEM and 3D Tera-Tom. The difference in SOR in water was large between$^{18}$F and$^{124}$I, it was about 0.88. $^{18}$F has higher SOR value when used Tera-Tomo algorithm or FPB algorithm, it was 1.0 and 0.95, respectively, while $^{89}$Zr and $^{124}$I have lower SORs values than $^{18}$F. For $^{89}$Zr, we found a reduction in SOR value when use Tera-Tom algorithm, it was 0.16 where it was about 0.2 when using FPB algorithm. These values were 0.12 and 0.16 respectively, for $^{124}$I. The difference in SORs in air field chamber are shown in (Figure 4a). (Figure 4b) illustrated the effect of the image reconstruction algorithms on the SORs values for each radionuclide. There were no significant variations in SORs values between $^{18}$F ,$^{89}$Zr and $^{124}$I when used Tera-Tomo reconstruction method, the SORs values were 0.15,0.17 and 0.16 for $^{18}$F ,$^{89}$Zr and $^{124}$I, respectively. In the case of using FBP reconstruction algorithm, the SORs values were increased for $^{18}$F and$^{89}$Zr, they were 0.23 for both $^{18}$F and$^{89}$Zr where the SOR value of $^{124}$I decreased by 52% as compared with $^{18}$F and $^{89}$Zr, it was 0.11 for $^{124}$I (Table 4). The attenuation and scatter correction were not used because it did not install on the system.

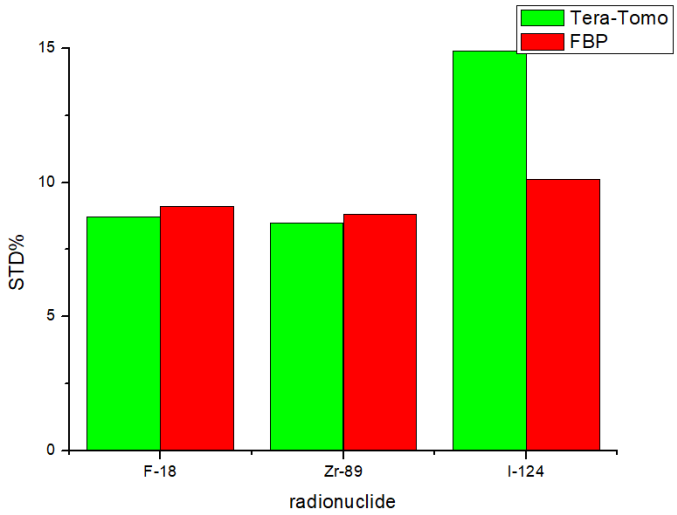


**Figure 4:** %SD in uniform phantom region of $^{18}F$, $^{89}Zr$ and $^{124}I$ with different reconstruction algorithm performed with no correction.

**Table 4:** The recovery coefficient(RC) values of 3 different isotopes.

| Recovery coefficient | | | | | | |
|---|---|---|---|---|---|---|
| **Tera-Tomo 3D-reconstruction** | | | | | | |
| **Rods** | **RC** | | | **%STDRC** | | |
| | **$F^{18}$** | **$Zr^{89}$** | **.$^{124}I$** | **$F^{18}$** | **$Zr^{89}$** | **.$^{124}I$** |
| 1 mm rod | 0.16 | 0.07 | 0.09 | 54.7 | 30.6 | 43.1% |
| 2 mm rod | 0.81 | 0.99 | 0.21 | 23.4 | 29.7 | 31.4% |
| 3 mm rod | 1.04 | 1.57 | 0.51 | 19.5 | 22.0 | 30.5% |
| 4 mm rod | 1.01 | 1.47 | 0.69 | 15.7 | 14.9 | 32.7% |
| 5 mm rod | 1.01 | 1.35 | 0.85 | 15.2 | 17.1 | 28.5% |
| **FBP 2D-reconstruction** | | | | | | |
| **Rods** | **RC** | | | **%STDRC** | | |
| | **$F^{18}$** | **$Zr^{89}$** | **.$^{124}I$** | **$F^{18}$** | **$Zr^{89}$** | **.$^{124}I$** |
| 1 mm rod | 0.15 | 0.18 | 0.08 | 29.4 | 41.5 | 37.0% |
| 2 mm rod | 0.54 | 0.91 | 0.20 | 11.3 | 29.6 | 35.9% |
| 3 mm rod | 0.75 | 1.26 | 0.44 | 12.9 | 31.6 | 21.9% |
| 4 mm rod | 0.76 | 1.23 | 0.60 | 11.3 | 20.5 | 22.0% |
| 5 mm rod | 0.88 | 1.30 | 0.83 | 11.2 | 22.2 | 24.3% |

## RCs

The RC values and (STD%) using 3D and 2D reconstruction are summarized , (Figure 5) represents the data. A significant difference was introduced for different radionuclides. The smallest values of RC were found for $^{124}I$ as compared to $^{18}F$ and $^{89}Zr$, but this variation not obtained for different reconstruction algorithms. A high reduction in RC value was observed for $^{18}F$ when used FBP reconstruction. $^{89}Zr$ has the highest value of RC in both cases of different reconstruction algorithms (Figure 6). The maximum difference was shown for 3 mm rod. In all results that discussed above, no attenuation or scatter corrections were used.

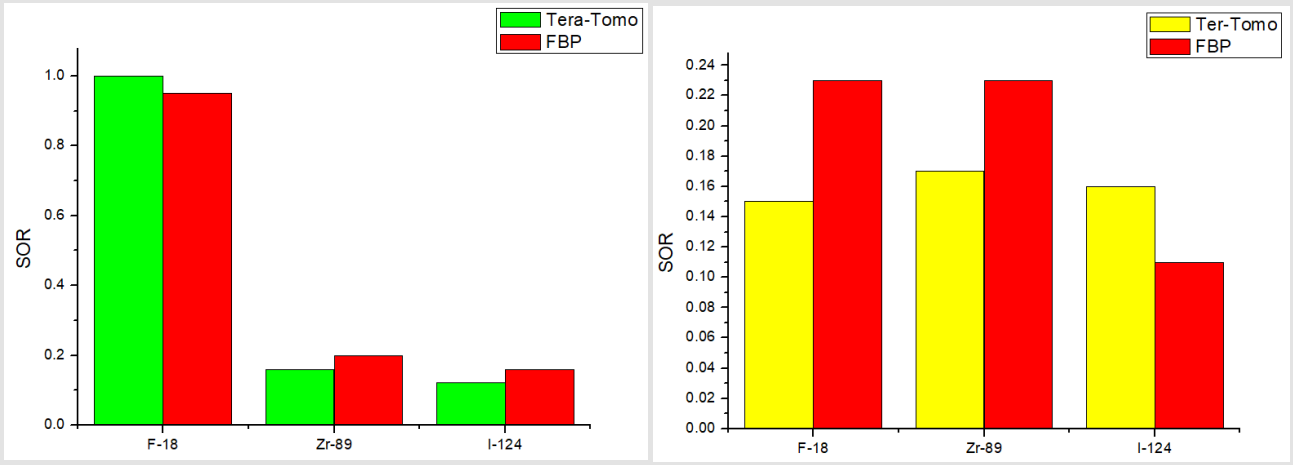


A B

**Figure 5:** SORs in
A. Water and
B. Air
compartments for various radionuclides, reconstructed with 2 different algorithms.

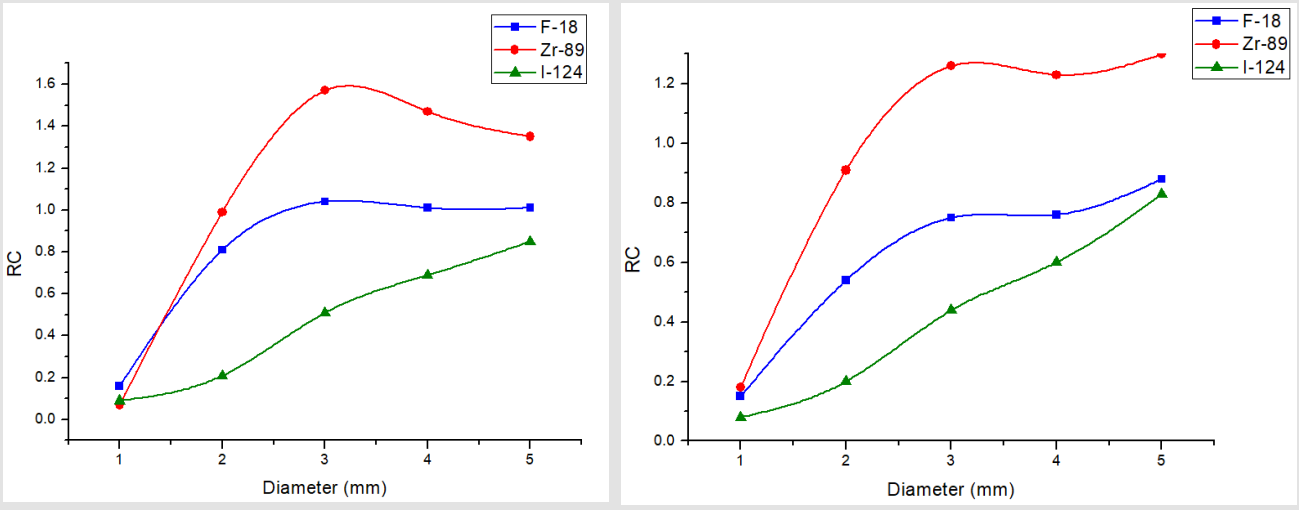


A B

**Figure 6:** RCs of different rods for various radionuclides, reconstructed with
A. Tera-Tomo and
B. FBP.

## Discussion

Several studies have studied the effective parameters on the image quality of some long-half-life positrons, such as $^{89}$Zr, $^{124}$I, and $^{68}$Ga. This study looks at the imaging properties of $^{124}$I and compares them to those of $^{18}$F when it is used with a small animal NanoScan® PET/CT scanner. As mentioned in the Lubberink study [10], positron energy is one of the most important factors affecting image resolution. He showed that $^{124}$I emits positrons with energies ranging from 686 to 973 Kev, while $^{18}$F emits positrons with a mean energy of 250 Kev and 89Zr with 389 Kev. This increase in positron energy of $^{124}$I results in a reduction in spatial resolution. On the other hand, The greater positron ranges of $^{124}$I, on the other hand, have an effect on spatial resolution, which is more severe in small animal PET than in human whole-body PET. The theoretical spatial resolution for small animal PET is 1.3 mm and 2.9 mm for $^{18}$F and I-124, respectively [10]. As expected, the results of the point source are consistent with previous studies. The positron range limits the spatial resolution in pre-clinical systems [3]. $^{124}$I, with a mean positron range of about 3.48 mm, has significantly low resolution (high value of FWHM) as compared with $^{89}$Zr and $^{18}$F. There was a 47.6% reduction. This is consistent with other studies, such as Liu

and Laforest's [11] study, which evaluated the resolution of 76Br using designed phantoms in a high-resolution small animal PET scanner and found that 76Br can achieve 2 mm of spatial resolution while $^{18}$F can only achieve 1.7 mm.

De Jong, et al. [11] have analyzed the imaging characteristics of $^{68}$Ga (Emax = 1.9 MeV, + range = 3.1 mm), $^{124}$I (Emax = 2.1 MeV, + range = 3.0 mm), and $^{89}$Zr (Emax = 0.9 MeV, + range = 1.23 mm), and they found that $^{18}$F has the best resolution of all isotopes investigated, followed by $^{89}$Zr, because of their relatively shorter positron range as compared to $^{68}$Ga and $^{124}$I [12]. Additionally, a study by Lee, et al. [13] showed that the spatial resolution of $^{124}$I was degraded by 19.9% compared to that of $^{18}$F on the ECAT HR+ scanner (Siemens Healthcare GmbH). Alanazi, et al. [4] have shown that there was a 2.2% decrease in spatial resolution measured at 1 cm off-axis for $^{89}$Zr in comparison with the obtained value of $^{18}$F Radial and tangential spatial resolution values measured at 10 cm off-axis have 2 and 4.1% reductions for $^{89}$Zr in comparison with $^{18}$F, respectively. This shows that $^{18}$F has a significantly higher resolution than $^{89}$Zr. The SOR values were the highest values in the water-filled compartment for $^{18}$F, while they were close to each other for $^{124}$I and $^{89}$Zr. On the other hand, in the case of an air-filled compartment, the results have shown no significant difference when Tera-Tomo 3D reconstruction was used. This may be because we did not use any correction, scatter, or attenuation. This can have caused the positrons emitted in the body part of the phantom to annihilate in the water-filled scatter compartment. The scatter and single photon have the main contribution to the SORs [4].

In a perfect system, the optimal limit of the recovery coefficients (RC) is supposed to equal 1. For both isotopes, the RCs discovered in this test had lower RC values when reconstructed using the 2D reconstruction algorithm than when reconstructed with the 3D reconstruction algorithm. For F-18 utilizing 2D, the RC values were approaching 1 for rods with a long diameter of 3 mm, 4 mm, and 5 mm, and about 1 for Zr-89. While for rods with diameters of 3 mm, 4 mm, and 5 mm, the RCs values determined using the 3D reconstruction algorithm exceeded 1 for both F-18 and Zr-89. When employing the 2D and 3D reconstruction algorithms, there was no significant difference in the RC values of I-124. This effect is known as the Gibbs effect [14]. These RC values match those published by Nagy [15] for NanoScan PET/MRI system rods with diameters of 1 mm and 2 mm. According to Goertzen [16], the RC values are highly dependent on the reconstruction algorithm. In addition, the prompt ɣ-photons for $^{124}$I and $^{89}$Zr have contributed to image noise and caused an increase in STD%. This appeared clearly in $^{124}$I. The results of RC values have shown the effect of positron range. A significant reduction was observed for $^{124}$I. These results are compatible with those obtained by Liu, et al. [17] where they found the RCs values of radionuclides which have a longer positron range, such as 61Cu and $^{68}$Ga, than $^{18}$F, were lower than the RCs values of $^{18}$F. The corrected RCs in medium and smallest spheres ranged from 75% to 90% for 61Cu and $^{68}$Ga, where s for $^{18}$F are close to 100%. Lubberink, et al. [10] investigated the effect of image resolution degradation for $^{124}$I on recovery, and they showed that recovery for $^{124}$I was considerably worse than for $^{124}$I, even for spheres as large as 37 mm in diameter.

## Conclusion

In this study, the image quality parameters and spatial resolution were evaluated for nonconventional radionuclides such as $^{124}$I and $^{89}$Zr using the small animal NanoScan® PET/CT scanner. The presence of prompt ɣ -photons and the higher positron range are two major issues that can limit image quality performance. The high differences in the SOR and significant reduction in RCs were observed for $^{124}$I as compared to $^{89}$Zr and $^{18}$F. The best results were found for $^{18}$F. The presence of ɣ -photons effects on the image quality parameters for the high positron range, particularly SD%. Due to the no-scatter correction being used, the single photon can contribute and cause some artifacts in the image. These artifacts can cause distortions in SOR and RC values.

## Disclosure

No potential conflict of interest relevant to this article was reported.

## References

1. Van Der Vos Charlotte S, Daniëlle Koopman, Sjoerd Rijnsdorp, Albert J Arends, Ronald Boellaard, et al. (2017) Quantification, improvement, and harmonization of small lesion detection with state-of-the-art PET. European journal of nuclear medicine and molecular imaging 44(1): 4-16.
2. Disselhort Jonathan A, Maarten Brom, Peter Laverman, Cornelius H Slump, Otto C Boerman, et al. (2010) Image-quality assessment for several positron emitters using the NEMA NU 4-2008 standards in the Siemens Inveon small-animal PET scanner. Journal of nuclear medicine 51(4): 610-617.
3. Szanda Istvan, Jane Mackewn, Gergely Patay, Peter Major, Kavitha Sunassee, et al. (2011) National Electrical Manufacturers Association NU-4 performance evaluation of the PET component of the NanoPET/CT preclinical PET/CT scanner. Journal of nuclear medicine 52(11): 1741-1747.
4. Alanazi Sitah F, Khalid S Alzimami, Magdy M Ghannam, Ibrahim J Aljammaz, Faisal Alrumayan, et al. (2016) Quantitative imaging characteristics of zirconium-89 on Gemini Time-Of-Flight PET/CT. Nuclear medicine communications 37(12): 1238-1245.
5. Van Den Winkel P (2004) Standardized high current solid targets for cyclotron production of diagnostic and therapeutic radionuclides. IAEA Vienna, p. 25-35.
6. W Severin Gregory, Jonathan W Engle, Todd E Barnhart, R Jerry Nickles (2011) 89Zr radiochemistry for positron emission tomography. Medicinal chemistry 7(5): 389-394.
7. Al Yanbawi S, Al Jammaz I (2007) Standardized high current solid tellurium-124 target for cyclotron production of the radionuclides iodine-123,124. Radiochimica Acta 95(11): 657-661.

8. Lee Young Sub, Jin Su Kim, Jung Young Kim, Byung Il Kim, Sang Moo Lim, et al. (2015) Spatial resolution and image qualities of Zr-89 on Siemens Biograph TruePoint PET/CT. Cancer Biotherapy and Radiopharmaceuticals 30(1): 27-32.

9. Palmer Matthew R, Zhu Xuping, Parker J Anthony (2005) Modeling and simulation of positron range effects for high resolution PET imaging. IEEE Transactions on Nuclear Science 52(5): 1391-1395.

10. Lubberink Mark, Herzog Hans (2011) Quantitative imaging of 124 I and 86 Y with PET. European journal of nuclear medicine and molecular imaging 38(1): 10-18.

11. De Jong Hugo Wam, L Perk, GWM Visser, R Boellaard, GAMS Van Dongen, et al. (2005) High resolution PET imaging characteristics of/sup 68/Ga, /sup 124/I and/sup 89/Zr compared to/sup 18/F. IEEE Nuclear Science Symposium Conference Record IEEE 3: 1624-1627.

12. LEE Young Sub, Jin Su Kim, Hee Joung Kim (2013) Imaging Characteristics of $^{124} $ I Between 3D and 2D on Siemens ECAT HR ${+} $ PET Scanner. IEEE Transactions on Nuclear Science 60(2): 797-801.

13. Dahle TJ (2014) Performance Evaluation of a Small-animal PET/CT System 2014.

14. Nagy K, Tóth M, Major P, Gergely Patay, Gyozo Egri, et al. (2013) Performance evaluation of the small-animal nanoScan PET/MRI system. J Nucl Med 54(10): 1825-1832.

15. Goertzen AL, Bao Q, Bergeron M, Eric Blankemeyer, Stephan Blinder, et al. (2012) NEMA NU 4-2008 comparison of preclinical PET imaging systems. J Nucl Med 53(8): 1300-1309.

16. Liu Xiaodong, Laforest Richard (2009) Quantitative small animal PET imaging with nonconventional nuclides. Nuclear medicine and biology 36(5): 551-559.

17. Laforest Richard, Liu Xiaodong (2009) Cascade removal and microPET imaging with 76Br. Physics in Medicine & Biology 54(6): 1503-1531.

**ISSN: 2574-1241**

DOI: 10.26717/BJSTR.2022.42.006749

**Sitah Fahad Alanazi.** Biomed J Sci & Tech Res



**Submission Link**: https://biomedres.us/submit-manuscript.php